Chapter 27
Model Order Reduction of Nonlinear Eddy Current Problems Using Missing Point Estimation

Y. Paquay, O. Brüls, and C. Geuzaine

Abstract In electromagnetics, the finite element method has become the most used tool to study several applications from transformers and rotating machines in low frequencies to antennas and photonic devices in high frequencies. Unfortunately, this approach usually leads to (very) large systems of equations and is thus very computationally demanding. This contribution compares three model order reduction techniques for the solution of nonlinear low frequency electromagnetic applications (in the so-called magnetoquasistatic regime) to efficiently reduce the number of equations—leading to smaller and faster systems to solve.

27.1 Introduction

The Finite Element (FE) method has been used in numerous engineering fields to simulate various phenomena, from structural analysis to combustion modelling to electromagnetics. While its main advantage is to correctly represent dynamical and nonlinear behaviours, the spatial discretization inherent to the FE method is also its main drawback, as it usually leads to (very) large systems of (nonlinear) equations. This extensive number of equations requires a lot of computational resources, usually far too much for quasi-real time simulations.

In this paper, we propose to apply a methodology that combines the Proper Orthogonal Decomposition (POD) [19] and the Missing Point Estimation (MPE) [2] to reduce those large FE systems for nonlinear eddy current applications, e.g. for the modeling of a 3-phase power transformer, to only dozens of equations—and therefore allowing a drastic reduction in the computational time and required

Y. Paquay (✉) • C. Geuzaine
Montefiore Institute, University of Liège, Allée de la découverte B28, B-4000 Liège, Belgium
e-mail: yannick.paquay@ulg.ac.be; cgeuzaine@ulg.ac.be

O. Brüls
Department of Aerospace and Mechanical Engineering, University of Liège, Allée de la dècouverte B52, B-4000 Liège, Belgium
e-mail: o.bruls@ulg.ac.be

P. Benner et al. (eds.), *Model Reduction of Parametrized Systems*,
MS&A 17, DOI 10.1007/978-3-319-58786-8_27

resources. This paper also presents a discussion on the use of the Discrete Empirical Interpolation Method (DEIM) [6] in the magnetoquasistatic case, which has already been efficiently used in the static case [7].

27.2 Eddy current problem

Let us consider a general spatial domain Ω (boundary Γ) where the nonlinear eddy current problem is to be solved in the time domain during T seconds with N_t equispaced timesteps—the corresponding time increment $\Delta t = T/N_t$. In this problem, the source is imposed directly as a current density $\mathbf{j}$ in a source domain $\Omega_j \subset \Omega$. This current density $\mathbf{j}$ generates a magnetic field $\mathbf{h}$ and a corresponding induction field $\mathbf{b} = \mu\mathbf{h}$ in Ω where μ is the permeability of the medium ($\mu = 1/\nu$ with ν the reluctivity). In general, Ω consists of linear and nonlinear magnetic subdomains, Ω^l and Ω^{nl} respectively. In Ω^l, the reluctivity is constant (e.g. $\nu = \nu_0$ with ν_0 the vacuum reluctivity) whereas in Ω^{nl} it depends on the induction field $\mathbf{b}$, i.e. $\nu = \nu(\mathbf{b})$. Parts $\Omega_c \subset \Omega$ ($\Omega_c \cap \Omega_j = \emptyset$) can be conducting with conductivity σ, in which induced currents will arise if $\mathbf{j}$ is time varying. The conductivity and the nonlinear reluctivity of a material are independent, e.g. a material can be conductive and nonlinear and would be written as Ω_c^{nl}.

The general nonlinear eddy current problem is derived from Maxwell's equations where displacement currents are neglected, and can be formulated in terms of the magnetic vector potential $\mathbf{a} \in \mathbf{H}(\mathbf{curl}, \Omega) \triangleq \left\{\mathbf{a} \in \mathbf{L}^2(\Omega); \mathbf{curl}\,\mathbf{a} \in \mathbf{L}^2(\Omega)\right\}$ such that $\mathbf{b} = \mathbf{curl}\,\mathbf{a}$ [4]:

$$\sigma\,\partial_t \mathbf{a} + \mathbf{curl}\,[\nu(\mathbf{curl}\,\mathbf{a})\,\mathbf{curl}\,\mathbf{a}] = \mathbf{j} \text{ in } \Omega, \tag{27.1}$$

$$\mathbf{a} \times \mathbf{n} = 0 \text{ in } \Gamma, \tag{27.2}$$

where $\mathbf{n}$ is the outer unit normal vector. Multiplying Eq. (27.1) by appropriate test functions and integrating by part over Ω leads to the following weak formulation: find $\mathbf{a}$ such that

$$\left(\sigma\,\partial_t \mathbf{a}, \mathbf{a}'\right)_{\Omega_c} + \left(\nu\mathbf{curl}\,\mathbf{a}, \mathbf{curl}\,\mathbf{a}'\right)_{\Omega} + \left\langle \mathbf{n} \times \nu\mathbf{curl}\,\mathbf{a}, \mathbf{a}'\right\rangle_{\Gamma} = \left(\mathbf{j}, \mathbf{a}'\right)_{\Omega_j} \tag{27.3}$$

holds for all test functions $\mathbf{a}' \in \mathbf{H}_0(\mathbf{curl}, \Omega) \triangleq \{\mathbf{a}' \in \mathbf{H}(\mathbf{curl}, \Omega);\, \mathbf{a}' \times \mathbf{n} = 0|_{\Gamma}\}$. The second term can be decomposed in the linear and nonlinear subdomains as

$$\left(\nu\mathbf{curl}\,\mathbf{a}, \mathbf{curl}\,\mathbf{a}'\right)_{\Omega} = \left(\nu_0\mathbf{curl}\,\mathbf{a}, \mathbf{curl}\,\mathbf{a}'\right)_{\Omega^l} + \left(\tilde{\nu}(\mathbf{curl}\,\mathbf{a})\mathbf{curl}\,\mathbf{a}, \mathbf{curl}\,\mathbf{a}'\right)_{\Omega^{nl}}. \tag{27.4}$$

Applying the standard Galerkin finite element method using Whitney edge elements [9] on Eq. (27.3) leads to the spatially discretized system of differential algebraic

equations [7]:

$$\mathbf{M}\dot{\mathbf{x}} + \mathbf{S}(\mathbf{x})\mathbf{x} = \mathbf{v}, \tag{27.5}$$

where $\mathbf{x}$ is the vector of unknowns of size N, $\mathbf{M}$ is the mass matrix that represents the dynamics, $\mathbf{S}$ is the magnetic stiffness matrix and $\mathbf{v}$ depends on the source current density $\mathbf{j}$.

Applying an implicit Euler scheme for the time discretisation of Eq. (27.5) leads to the discrete system of equations at time $t_k = k\Delta t$ for $k = 1, \cdots, N_t$:

$$\left[\frac{\mathbf{M}}{\Delta t} + \mathbf{S}(\mathbf{x}_k)\right]\mathbf{x}_k = \frac{\mathbf{M}}{\Delta t}\mathbf{x}_{k-1} + \mathbf{v}_k \tag{27.6}$$

with $\mathbf{x}_k = \mathbf{x}(t_k)$ and $\mathbf{v}_k = \mathbf{v}(t_k)$.

A Newton-Raphson (NR) scheme is used to linearize Eq. (27.6) at each time step. To this end, starting from an initial guess $\mathbf{x}_k^0 = \mathbf{x}_{k-1}$ and $\mathbf{x}_0^0 = \mathbf{0}$, the linear system

$$\mathbf{J}(\mathbf{x}_k^i)\delta\mathbf{x}_k^i = \mathbf{r}(\mathbf{x}_k^i) \tag{27.7}$$

is solved and the solution is updated with

$$\mathbf{x}_k^{i+1} = \mathbf{x}_k^i + \delta\mathbf{x}_k^i \tag{27.8}$$

for $i = 1, \cdots, n$ such that $\left\|\delta\mathbf{x}_k^n\right\|_2 \leq 10^{-5}$, i.e. until the increment is sufficiently small, at which point $\mathbf{x}_k$ is taken as $\mathbf{x}_k^n$. In Eq. (27.7), $\mathbf{J}(\mathbf{x}_k^i)$ is the Jacobian matrix depending on $\mathbf{x}_k^i$ and $\mathbf{r}_k^i$ is the residual given by

$$\mathbf{r}(\mathbf{x}_k^i) = \frac{\mathbf{M}}{\Delta t}\mathbf{x}_{k-1} + \mathbf{v}_k - \left[\frac{\mathbf{M}}{\Delta t} + \mathbf{S}(\mathbf{x}_k^i)\right]\mathbf{x}_k^i. \tag{27.9}$$

27.3 Model Order Reduction

The size of Eq. (27.7) equals the size N of the unknown vector $\mathbf{x}$, which can be (very) large for practical engineering simulations. This section aims at defining successful techniques to reduce the system size (and thus the CPU time required to obtain the solution). Three methods are considered: the Proper Orthogonal Decomposition (POD) [18], the Discrete Empirical Interpolation Method (DEIM) [6] and the Missing Point Estimation (MPE) [2].

27.3.1 Proper Orthogonal Decomposition

The POD is applied to reduce the system of Eq. (27.6) or the NR system from Eq. (27.7) by using a snapshot matrix $\mathbf{X}$ [19] that gathers the solutions for all time steps (called snapshots):

$$\mathbf{X} = \left[\mathbf{x}_1, \mathbf{x}_2, \cdots, \mathbf{x}_{N_t} \right] \in \mathbf{R}^{N \times N_t} \tag{27.10}$$

where N_t is the number of time steps. Contrary to [7] where the calculation of the SVD is made using the covariance matrix (i.e. $\mathbf{X}^T\mathbf{X}$), we directly perform a thin singular value decomposition (SVD) on the snapshot matrix $\mathbf{X}$—maintaining the same efficiency but without computing the covariance matrix. Then

$$[\mathbf{U}_x, \Xi_x, \mathbf{V}_x] = \text{thin svd}(\mathbf{X}) \tag{27.11}$$

and the reduced basis is given by $\mathbf{U}_x$. The vector $\mathbf{x} \in \mathbf{R}^{N \times 1}$ is reduced in the basis $\mathbf{U}_x$ to a vector $\tilde{\mathbf{x}} \in \mathbf{R}^{r \times 1}$ ($r \ll N$):

$$\mathbf{x} = \mathbf{U}_x \tilde{\mathbf{x}}. \tag{27.12}$$

The reduced solution $\tilde{\mathbf{x}}$ obtained by projecting $\mathbf{x}$ onto the reduced basis $\mathbf{U}_x$ given by the application of the SVD on a snapshot matrix has been shown as the optimal (best) choice [21]. At this point, r equals N_t and in typical cases $N_t \ll N$. Nevertheless, from [21], we could also truncate the reduced basis $\mathbf{U}_x$ to its $r < N_t$ first columns in order to approximate the original snapshot matrix with a given error ε_r. Similarly, the reduced basis $\mathbf{U}_x$ could be truncated based on the Kolmogorov r-width K_r, which measures the extent to which $\mathbf{X}$ can be approximated by a r-dimensional subspace of a normed linear space [8, 13, 14]. In practice, K_r and ε_r decrease monotonically with r. Thanks to the singular values, the error ε_r is computed as:

$$\varepsilon_r = \frac{\sum_{i=r+1}^{n} \xi_i^2}{\sum_{i=1}^{n} \xi_i^2} \tag{27.13}$$

where ξ_i is the ith singular value in the diagonal of Ξ_x. The lower ε_r (e.g. $\varepsilon_r \leq 10^{-8}$), the better; graphically, this indicator measures the decay of the singular values: the fastest, the better.

By injecting Eq. (27.12) into Eq. (27.6), the reduced system is overdetermined with N equations for r unknowns:

$$\left[\frac{\mathbf{M}}{\Delta t} + \mathbf{S}(\mathbf{U}_x \tilde{\mathbf{x}}_k) \right] \mathbf{U}_x \tilde{\mathbf{x}}_k = \frac{\mathbf{M}}{\Delta t} \mathbf{U}_x \tilde{\mathbf{x}}_{k-1} + \mathbf{v}_k \tag{27.14}$$

and by applying a Galerkin projection onto the same reduced basis [21], the reduced system becomes:

$$\left[\frac{\tilde{\mathbf{M}}}{\Delta t} + \tilde{\mathbf{S}}(\mathbf{U}_x\tilde{\mathbf{x}}_k)\right]\tilde{\mathbf{x}}_k = \frac{\tilde{\mathbf{M}}}{\Delta t}\tilde{\mathbf{x}}_{k-1} + \tilde{\mathbf{v}}_k \tag{27.15}$$

where $\tilde{\mathbf{M}} = \mathbf{U}_x^T\mathbf{M}\mathbf{U}_x$ (similarly for $\tilde{\mathbf{S}}$) and $\tilde{\mathbf{v}}_k = \mathbf{U}_x^T\mathbf{v}_k$. By analogy for the NR method, Eq. (27.7) becomes

$$\tilde{\mathbf{J}}(\tilde{\mathbf{x}}_k^i)\delta\tilde{\mathbf{x}}_k^i = \tilde{\mathbf{r}}(\tilde{\mathbf{x}}_k^i) \tag{27.16}$$

with the corresponding reduced matrices

$$\tilde{\mathbf{J}}(\tilde{\mathbf{x}}_k^i) = \mathbf{U}_x^T\mathbf{J}(\mathbf{U}_x\tilde{\mathbf{x}}_k^i)\mathbf{U}_x, \tag{27.17}$$

$$\tilde{\mathbf{r}}(\tilde{\mathbf{x}}_k^i) = \frac{\tilde{\mathbf{M}}}{\Delta t}\tilde{\mathbf{x}}_{k-1} + \tilde{\mathbf{v}}_k - \left[\frac{\tilde{\mathbf{M}}}{\Delta t} + \tilde{\mathbf{S}}(\mathbf{U}_x\tilde{\mathbf{x}}_k^i)\right]\tilde{\mathbf{x}}_k^i. \tag{27.18}$$

The size of the reduced system of Eq. (27.16) is $r \ll N$ as expected but the nonlinear parts in Eqs. (27.17) and (27.18) (i.e. $\tilde{\mathbf{S}}(\mathbf{U}_x\tilde{\mathbf{x}}_k^i)$ and $\tilde{\mathbf{J}}(\mathbf{U}_x\tilde{\mathbf{x}}_k^i)$) still depend on the full order solution $\mathbf{x}_k^i = \mathbf{U}_x\tilde{\mathbf{x}}_k^i$. Therefore the evaluation of these terms still requires to expand the reduced states to the full order size solution at each nonlinear iteration.

27.3.2 Discrete Empirical Interpolation Method

The DEIM [6] (or its continuous version EIM [3]) is a nonlinear reduction technique that projects a few evaluations of a large vector (or matrix) onto a smaller mapping basis in order to reduce the computational time originally required to generate it. Let us consider the large vector $\mathbf{z}(\mathbf{p}) \in \mathbf{R}^{N\times 1}$ depending on some parameters $\mathbf{p}$ and construct the snapshot matrix $\mathbf{Z}$ as:

$$\mathbf{Z} = \left[\mathbf{z}(\mathbf{p}_1), \mathbf{z}(\mathbf{p}_2), \cdots\right]. \tag{27.19}$$

One would like to write

$$\mathbf{z}(\mathbf{p}) \simeq \mathbf{U}_z\bar{\mathbf{z}}(\mathbf{p}) \tag{27.20}$$

where $\mathbf{U}_z \in \mathbf{R}^{N\times q}$ is a mapping basis and $\bar{\mathbf{z}}(\mathbf{p}) \in \mathbf{R}^{q\times 1}$ a reduced evaluation of $\mathbf{z}(\mathbf{p})$ with $q \ll N$. The matrix $\mathbf{U}_z$ is computed as the reduced basis $\mathbf{U}_x$ in Sect. 27.3.1 by applying a thin SVD on the snapshot matrix $\mathbf{Z}$ (and can be truncated by analyzing the singular values decay in Ξ_z):

$$[\mathbf{U}_z, \Xi_z, \mathbf{V}_z] = \text{thin svd}(\mathbf{Z}) \tag{27.21}$$

The DEIM expresses $\bar{\mathbf{z}}$ from the evaluation of only q components of $\mathbf{z}$ such that

$$\bar{\mathbf{z}}(\mathbf{p}) \simeq \left(\mathbf{P}^T\mathbf{U}_z\right)^{-1}\mathbf{P}^T\mathbf{z}(\mathbf{p}) \tag{27.22}$$

with $\mathbf{P} \in \mathbf{R}^{N\times q}$ a selection matrix for the q rows of $\mathbf{z}(\mathbf{p})$ which is found by applying the DEIM algorithm [6]. Here are the main steps of this procedure:

1. From Eq. (27.20), multiplying both sides by $\mathbf{P}^T$ to select q rows of $\mathbf{z}(\mathbf{p})$ leads to:

$$\mathbf{P}^T\mathbf{z}(\mathbf{p}) \simeq \left(\mathbf{P}^T\mathbf{U}_z\right)\bar{\mathbf{z}}(\mathbf{p}). \tag{27.23}$$

2. If $\left(\mathbf{P}^T\mathbf{U}_z\right)$ is invertible, then we can deduce the expression of $\bar{\mathbf{z}}(\mathbf{p})$ (Eq. 27.22) as:

$$\bar{\mathbf{z}}(\mathbf{p}) = \left(\mathbf{P}^T\mathbf{U}_z\right)^{-1}\mathbf{P}^T\mathbf{z}(\mathbf{p}). \tag{27.24}$$

3. Finally, by injecting Eq. (27.24) into Eq. (27.20), we obtain:

$$\mathbf{z}(\mathbf{p}) \simeq \mathbf{U}_z\left(\mathbf{P}^T\mathbf{U}_z\right)^{-1}\mathbf{P}^T\mathbf{z}(\mathbf{p}). \tag{27.25}$$

4. Since a FE element only depends on its neighbours (e.g. local influence), we can restrict the computations to these q local components without generating the overall vector $\mathbf{z}(\mathbf{p})$ (similarly with rows for matrices). Equation (27.25) can therefore be written as:

$$\mathbf{z}(\mathbf{p}) \simeq \mathbf{U}_z\left(\mathbf{P}^T\mathbf{U}_z\right)^{-1}\mathbf{z}(\mathbf{P}^T\mathbf{p}). \tag{27.26}$$

In the magnetoquasistatic case from Eqs. (27.17) and (27.18), the vectors $\tilde{\mathbf{S}}(\mathbf{U}_x\tilde{\mathbf{x}}_k^i)\tilde{\mathbf{x}}_k^i$ and $\tilde{\mathbf{J}}(\mathbf{U}_x\tilde{\mathbf{x}}_k^i)\tilde{\mathbf{x}}_k^i$ perfectly match the expression of $\mathbf{z}(\mathbf{p})$. Indeed, these vectors need to evaluate $\mathbf{S}(\mathbf{x}_k^i)$ and $\mathbf{J}(\mathbf{x}_k^i)$ respectively at each nonlinear iteration. By applying the DEIM with $\mathbf{z}(\mathbf{p}_k) = \mathbf{S}(\mathbf{x}_k^n)\mathbf{x}_k^n$, these expressions read:

$$\mathbf{S}(\mathbf{x}_k^i) \simeq \mathbf{U}_z\left(\mathbf{P}^T\mathbf{U}_z\right)^{-1}\mathbf{S}(\mathbf{P}^T\mathbf{x}_k^i), \tag{27.27}$$

$$\mathbf{J}(\mathbf{x}_k^i) \simeq \underbrace{\mathbf{U}_z\left(\mathbf{P}^T\mathbf{U}_z\right)^{-1}}_{\mathbf{U}_z^*}\mathbf{J}(\mathbf{P}^T\mathbf{x}_k^i), \tag{27.28}$$

where $\mathbf{U}_z^* \in \mathbf{R}^{N\times q}$ can be computed once. By injecting Eq. (27.27) in Eq. (27.18), the reduced residual becomes:

$$\tilde{\mathbf{r}}(\tilde{\mathbf{x}}_k^i) \simeq \frac{\tilde{\mathbf{M}}}{\Delta t}\tilde{\mathbf{x}}_{k-1} + \tilde{\mathbf{v}}_k - \left[\frac{\tilde{\mathbf{M}}}{\Delta t} + \mathbf{U}_x^T\mathbf{U}_z^*\mathbf{S}(\mathbf{P}^T\mathbf{U}_x\tilde{\mathbf{x}}_k^i)\mathbf{U}_x\right]\tilde{\mathbf{x}}_k^i. \tag{27.29}$$

As will be seen later in Sect. 27.4.2, the combination of POD with DEIM lacks robustness for the considered nonlinear eddy current problem. As an alternative, we investigate below the use of the Missing Point Estimation technique [2].

27.3.3 Missing Point Estimation

The MPE approach [2] has the same goal as the DEIM: reducing the computation of all entries of a general (nonlinear) vector or matrix. While the DEIM can be used alone to approximate a vector $\mathbf{z}$ based on a small set of evaluations projected onto a reduced basis $\mathbf{U}_z$ computed from (nonlinear) snapshots $\mathbf{Z}$ of the full size vector $\mathbf{z}$, the MPE must be combined with the POD since it replaces the projection subspace $\mathbf{U}_x^T$ by another subspace defined as $\mathbf{U}_x^T\mathbf{P}\mathbf{P}^T$. As a consequence, the reduction procedure follows a Petrov-Galerkin approach with different left and right projection subspaces. Other techniques use the same philosophy, e.g. Hyper-Reduction [17] or Gappy POD [5], and differ in the determination of the reduced number of evaluations.

Let us consider the term $\tilde{\mathbf{S}}(\mathbf{x}_k^i) = \mathbf{U}_x^T\mathbf{S}(\mathbf{x}_k^i)\mathbf{U}_x$ with $\mathbf{S}(\mathbf{x}_k^i)$ that still depends on the full size order solution $\mathbf{x}_k^i$. Applying the MPE on $\mathbf{S}(\mathbf{x}_k^i)$ gives a reduced set of its rows $\bar{\mathbf{S}}(\mathbf{x}_k^i)$:

$$\bar{\mathbf{S}}(\mathbf{x}_k^i) = \mathbf{P}^T\mathbf{S}(\mathbf{x}_k^i) \tag{27.30}$$

with $\mathbf{P} \in \mathbf{R}^{N\times q}$ ($q \ll N$) a selection matrix that gathers q rows of $\mathbf{S}$ (as previously explained, only the q rows of $\mathbf{S}$ are computed, i.e. $\mathbf{S}(\mathbf{P}^T\mathbf{x}_k^i)$). Since q rows are selected in $\mathbf{S}$, only the corresponding q rows in the POD basis are useful and then kept:

$$\bar{\mathbf{U}}_x = \mathbf{P}^T\mathbf{U}_x \tag{27.31}$$

with $\bar{\mathbf{U}}_x \in \mathbf{R}^{q\times r}$ computed once (or offline). By applying the MPE on Eq. (27.16) it reads:

$$\bar{\mathbf{U}}_x^T\bar{\mathbf{J}}(\mathbf{x}_k^i)\mathbf{U}_x\delta\tilde{\mathbf{x}}_k^i = \bar{\mathbf{U}}_x^T\bar{\mathbf{r}}(\mathbf{x}_k^i) \tag{27.32}$$

with $\bar{\mathbf{J}}(\mathbf{x}_k^i) = \mathbf{P}^T\mathbf{J}(\mathbf{x}_k^i) = \mathbf{J}(\mathbf{P}^T\mathbf{x}_k^i)$ and $\bar{\mathbf{r}}(\mathbf{x}_k^i) = \mathbf{P}^T\mathbf{r}(\mathbf{x}_k^i) = \mathbf{r}(\mathbf{P}^T\mathbf{x}_k^i)$. The overall system is reduced to an r-dimensional subspace (with the application of the POD basis $\mathbf{U}_x$) but only by considering q components of the FE model (using $\mathbf{P}$) with $r, q \ll N$. Contrary to the DEIM greedy algorithm which selects the points based on the snapshots matrix $\mathbf{Z}$, the MPE greedy algorithm tends to verify

$$\bar{\mathbf{U}}_x^T\bar{\mathbf{U}}_x \approx I \tag{27.33}$$

by increasing sequentially q with the most contributing rows [2] (this procedure may be long and should be done during an offline stage). While the DEIM strongly depends on the number of snapshots to determine the reduced set of unknowns, the MPE considers the original N FE degrees of freedom. In the worst case, $q = N_t$ with the DEIM and may be too small to correctly represent the nonlinear vector/matrix or $q = N$ with the MPE and all the degrees of freedom are taken into account. The selection is based on the criteria of Eq. (27.33) and can be equivalently seen as the decay of the condition number of $\bar{\mathbf{U}}_x^T \bar{\mathbf{U}}_x$ to 1. The closest the condition number is to 1, the better the criteria is fulfilled.

27.4 Numerical Results

As a test case, we consider a 2-D nonlinear model of a 3-phase power transformer such as depicted in Fig. 27.1 [10]. The model has $N = 7300$ unknowns and is simulated at no load. The nonlinear core reluctivity is given by the Brauer law:

$$\nu(\mathbf{b}) = \gamma + \alpha \exp(\beta \mathbf{b}^2) \tag{27.34}$$

with $\gamma = 80.47, \alpha = 0.05$ and $\beta = 4.21$ (from core material V330-50A [10]). The (laminated) core conductivity is either chosen as zero (nonconducting) or as

$$\sigma = \frac{d^2}{12}\sigma_{\text{iron}} = 4.16 \cdot 10^{-1}\ \text{S/m} \tag{27.35}$$

where d is the thickness of the laminations (0.5 mm) and $\sigma_{\text{iron}} = 2 \cdot 10^7$ S/m [11]. A single period at 50 Hz ($T = 20$ ms) with $N_t = 20$ time steps is analyzed and the input current density is given for phase i by:

$$\mathbf{j} = (-1)^{\eta} \frac{I}{S_c} \cos(2\pi f t + \phi_i)\hat{\mathbf{e}}_z \tag{27.36}$$

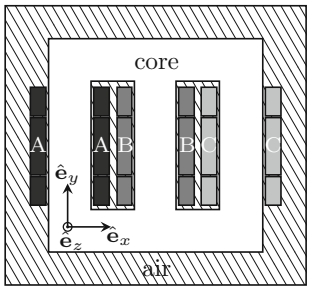

Fig. 27.1 FE model of the 3-phase transformer

Table 27.1 Subdomains of the 3-phase transformer in Fig. 27.1

Domain	Physical region	Legend in Fig. 27.1
$\Omega_c^{nl} \setminus \Omega_j$	Core (if $\sigma \neq 0$)	White
Ω_{cc}^{l}	Air	Lined
Ω_{cc}^{nl}	Core (if $\sigma = 0$)	White
Ω_j	Windings	Filled

Phase	Phase delay ϕ [rad]	Legend in Fig. 27.1
A	0	Black
B	$4\pi/3$	Gray
C	$2\pi/3$	Light gray

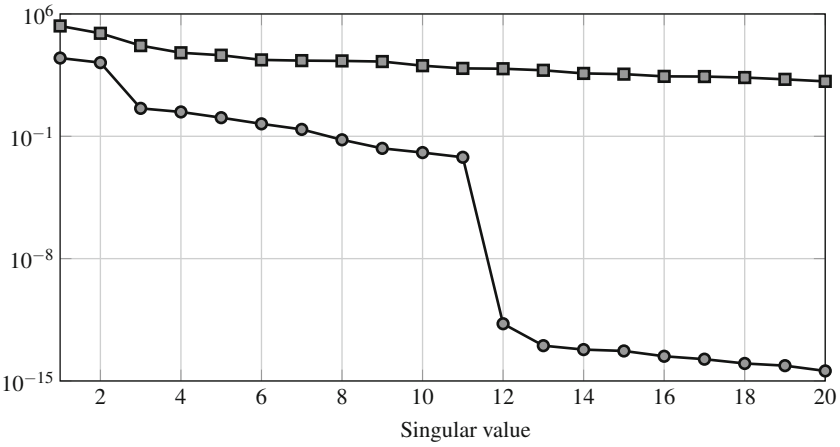

Fig. 27.2 Singular values of snapshot matrix $\mathbf{X}$, i.e. Ξ_x (*circled with line*) and snapshot matrix $\mathbf{Z}$, i.e. Ξ_z (*squared with line*) with $I = 0.3$ A & $\sigma = 4.16 \cdot 10^{-1}$ S/m

where $\eta = 0$ (resp. $\eta = 1$) for left (resp. right) part of the coil (representing the direction of the current), $I \in [0.1, 0.3]$ is the input peak current ($I = 0.1$ A induces linear magnetic behaviour whereas $I = 0.3$ A causes the core to saturate, see Fig. 27.9), S_c the coil surface, ϕ_i the phase delay of phase i and $\hat{\mathbf{e}}_z$ the unit vector along the z-axis. A full-order time domain simulation of 20 ms takes around 1 min to compute. The subdomains description is given in Table 27.1.

27.4.1 Proper Orthogonal Decomposition

First, in the reduction process, one must verify that the problem can be mapped onto a smaller r-dimensional subspace. Since the singular values of the snapshot matrix $\mathbf{X}$ quickly decay (circled with line in Fig. 27.2), the POD can indeed be used to reduce the system while preserving a small error. In the following tests, the POD

basis is truncated after the 11th singular value to fulfill $\varepsilon_r = 10^{-15}$ with $r = 11$. As explained in [16] for an inductor-core system, varying the input current does not always require to recompute the POD basis if the model is well trained with an appropriate current to correctly capture the nonlinear behaviour. By defining the reduced snapshot matrix $\tilde{\mathbf{X}}$ as:

$$\tilde{\mathbf{X}} = \left[\tilde{\mathbf{x}}_1, \tilde{\mathbf{x}}_2, \cdots, \tilde{\mathbf{x}}_{N_t} \right] \in \mathbf{R}^{r \times N_t}, \tag{27.37}$$

and using Eq. (27.12), we define the relative error of method i as:

$$\gamma_i = \frac{\left\| \mathbf{X} - \mathbf{U}_x \tilde{\mathbf{X}}_i \right\|_2}{\|\mathbf{X}\|_2}, \tag{27.38}$$

where $\tilde{\mathbf{X}}_i$ collects the reduction states obtained by reduction technique i. In this 3-phase transformer, a single POD basis can achieve a small relative error for all input currents—below 5% from an engineering point of view (dashed line in Fig. 27.3). Unfortunately, the perfect choice of that basis is very sensitive. Secondly, changing the conductivity value requires another POD basis due to a change in the eddy current distribution—similar to a change in frequency [16] (straight line in Fig. 27.4). For practical applications though, contrary to the input current, once the transformer is built, the conductivity is fixed and is no longer a parameter. If a local

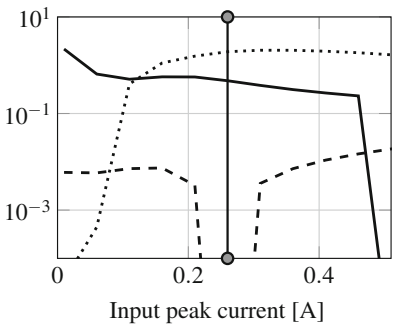

Fig. 27.3 Relative error γ_{POD} according to input peak current (basis generated with input current $I = 0.01$ A *dotted line*, 0.25 A *dashed line*, 0.5 A *straight line*). *Circled with line* represents the transition between linear and nonlinear regimes

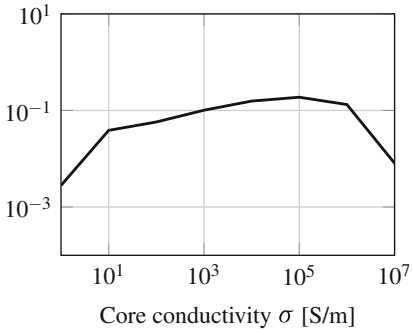

Fig. 27.4 Relative error γ_{POD} according to core conductivity (basis generated with $\sigma = 1$ S/m)

basis cannot correctly represent all the dynamics in a single low dimensional space, one would build a global basis by gathering all the snapshots of all parameter values [7] or interpolate between the local reduced bases in the parameter space [1, 16].

The POD reduces the magnetoquasistatic case to 11 equations leading to a theoretical speedup between 663 and 440,413 (the computational time plummets to between 90 and 0.1 ms) depending on the linear solver [12]. But the nonlinear terms still need the full order size: much of the computational gain is lost there, and the application of the POD alone is thus not sufficient.

27.4.2 Discrete Empirical Interpolation Method

In [7], the POD-DEIM has been used to efficiently reduce a static ($\sigma = 0$ S/m) 3D 3-phase transformer with an error lower than 0.1% by using 55 DEIM components (representing edges in the model). Once the core conductivity is no longer zero, however, the stability of the DEIM suffers and becomes more and more dependent on a priori independent parameters such as the number of time steps N_t or the conductivity σ [15, 20]. An alternative to the original DEIM algorithm is proposed in [22], i.e. DIME, but also presents the same issues in this eddy current problem (3-phase transformer, $I = 0.3$ A and $\sigma = 4.16 \cdot 10^{-1}$ S/m). This lack of robustness is illustrated in Figs. 27.5 and 27.6 where changing the number of time steps highly impacts the relative error obtained with the POD-DEIM squared with line and POD-DIME squared with dashed line techniques whereas the POD-MPE straight line approach keeps a quasi constant relative error. In Fig. 27.5, the DEIM/DIME reduced size q is obtained by truncating the nonlinear basis $\mathbf{U}_z$ through the SVD to maintain $\varepsilon \leq 10^{-15}$. In practice, the 25 first modes are significant (i.e. when $N_t \geq 25$). In Fig. 27.6, no truncation is performed on $\mathbf{U}_z$ and $q = N_t$. The results remain unchanged for $N_t > 90$. In both figures, the MPE reduced size is kept constant as the influence of the MPE reduced size on the error is analysed in Fig. 27.8 in the following section. By looking at the singular values of the nonlinear

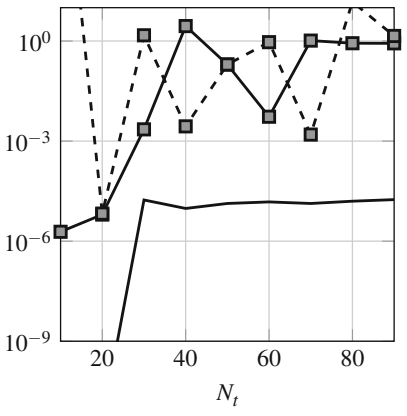

Fig. 27.5 Relative errors $\gamma_{\text{POD-DEIM}}$ (*squared with line*), $\gamma_{\text{POD-DIME}}$ (*squared with dashed line*) with $q = \min(25, N_t)$ and $\gamma_{\text{POD-MPE}}$ (*straight line*)

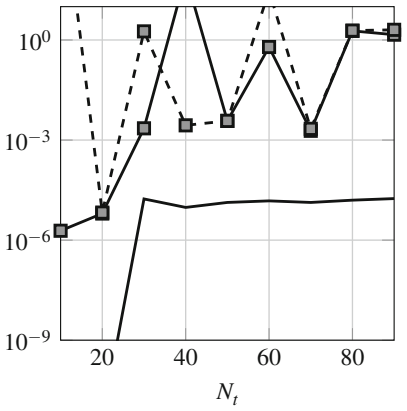

Fig. 27.6 Relative errors $\gamma_{\text{POD-DEIM}}$ (*squared with line*), $\gamma_{\text{POD-DIME}}$ (*squared with dashed line*) with $q = N_t$ and $\gamma_{\text{POD-MPE}}$ (*straight line*)

contribution, one can find a decay similar to the one depicted by squared with line in Fig. 27.2 where a small projection error is not achievable with a low number of modes (or similarly the Kolmogorov q-width is too large) to effectively represent the nonlinear term onto a q-dimensional subspace with $q \ll N$. Consequently, the POD-DEIM (and POD-DIME) can not correctly be used to reduce the computation of the nonlinear terms.

27.4.3 Missing Point Estimation

The application of the MPE consists in the determination of the q rows to keep in Eq. (27.16) to obtain Eq. (27.32). Contrary to the DEIM, it can be seen in Fig. 27.5 that the number of time steps N_t does not significantly influence the reduction. Similar results were obtained by varying the number of simulated periods T or the conductivity.

The POD-MPE is applied to the same 3-phase power transformer as the POD-DEIM (Fig. 27.1), using both the small ($I = 0.1$ A) and the large ($I = 0.3$ A) current values and either a zero ($\sigma = 0$ S/m) or nonzero ($\sigma = 4.16 \cdot 10^{-1}$ S/m) conductivity for the core. The condition number of $\bar{\mathbf{U}}_x^T \bar{\mathbf{U}}_x$, for both extreme cases, decays very fast to 1 (see Fig. 27.7). However, the relative error $\gamma_{\text{POD-MPE}}$ with respect to the reduction ratio seems to be independent of this criteria (see Fig. 27.8) where q ranges from 50 to 350 (depending on the configuration) for a relative error below 0.1%. This important reduction allows a high gain in the computational time and resources but a better criterion should be investigated. By applying the POD-MPE, the assembly of the nonlinear terms is limited to $q \in [50, \cdots, 350]$ rows instead of $N = 7300$ and the projection of them onto the reduced basis $\mathbf{U}_x$ at each nonlinear iteration is also computed faster compared to the original matrix products. The reduction ratios are comprised between 99% and 95% allowing a computational time from 0.6 to 3 s, still limited by the assembly time compared to the resolution time of 90 ms (obtained with the use of the POD allowing a drastic reduction to

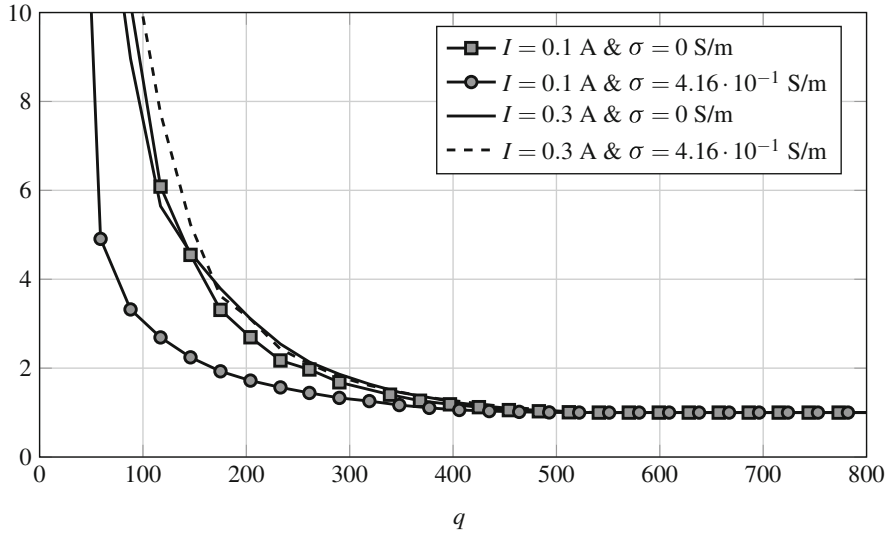

Fig. 27.7 Condition number of $\bar{\mathbf{U}}_x^T \bar{\mathbf{U}}_x$

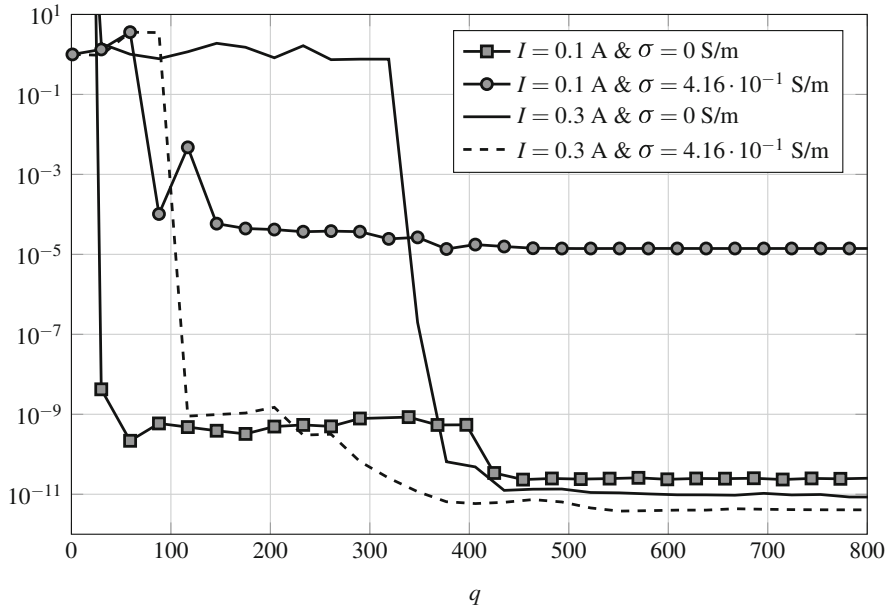

Fig. 27.8 Relative error $\gamma_{\text{POD-MPE}}$

$r = 11$). The induction field $\mathbf{b}$ for the different setups, i.e. $I = 0.1$ A (top)—$I = 0.3$ A (middle) and $\sigma = 0$ S/m (left)—$\sigma = 4.16 \cdot 10^{-1}$ S/m (right), and the MPE selected points (bottom) are shown in Fig. 27.9.

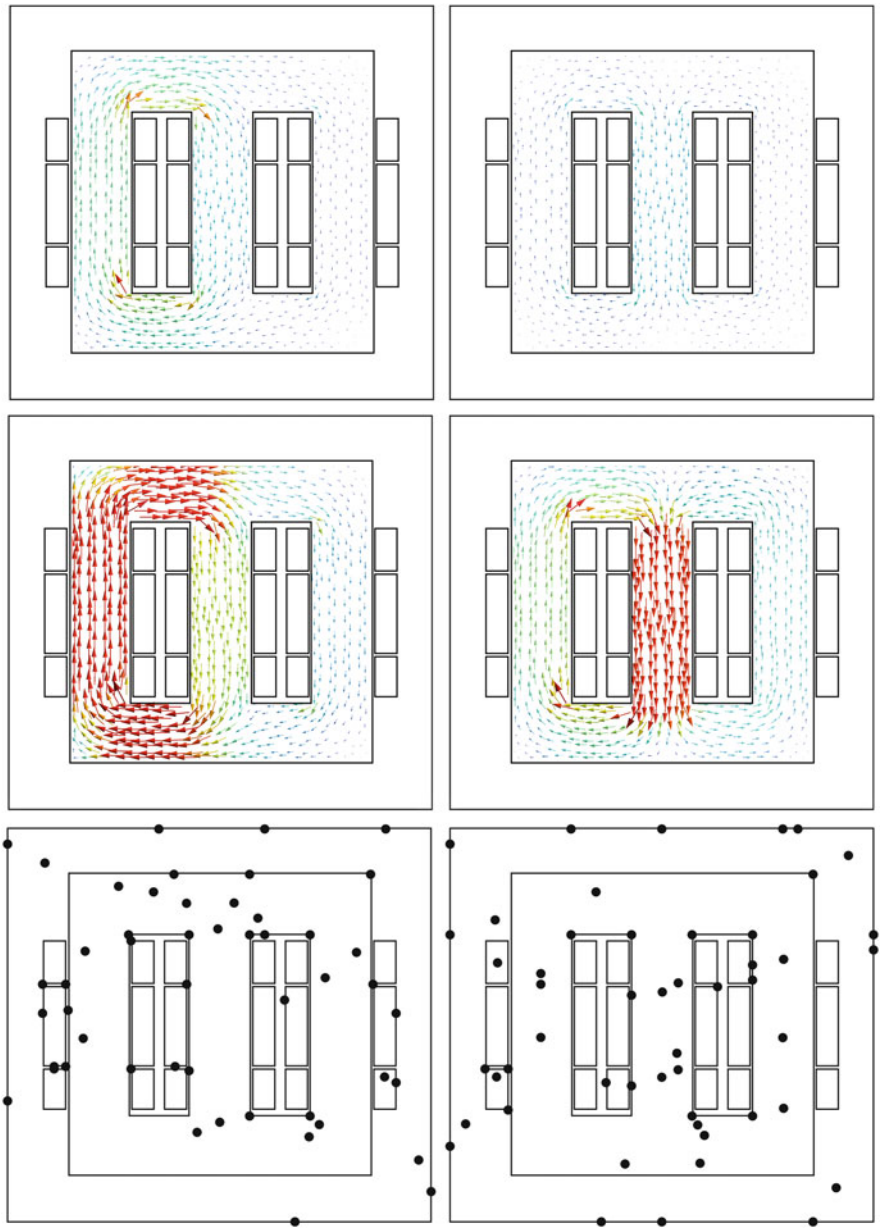

Fig. 27.9 20th time step of induction field **b** for $I = 0.1$ A (*top*) - $I = 0.3$ A (*middle*) and $\sigma = 0$ S/m (*left*) - $\sigma = 4.16 \cdot 10^{-1}$ S/m (*right*). Legend: linear scale from 0 T (*blue-small arrows*) to 1.52 T (*red-large arrows*) . 50 first MPE points (*bottom*)

27.5 Conclusion

In this paper, we investigated a combined approach of the Proper Orthogonal Decomposition and the Missing Point Estimation to efficiently and drastically reduce both nonlinear static and eddy current models of a 3-phase power transformer. The reduction ratios, comprised between 99% and 95% for the assembly and around 99.9% for the resolution, allow a reduced computational time of 0.6–5 s compared to the original finite element model resolution time of about 60 s. However, further work should investigate a better suited criterion on the a priori reduced size to ensure a sufficiently small error.

Acknowledgements This work was funded in part by the Belgian Science Policy under grant IAP P7-02 (Multiscale Modelling of Electrical Energy Systems) and by the F.R.S.—FNRS (Belgium).

References

1. Amsallem, D.: Interpolation on manifolds of CFD-based fluid and finite element-based structural reduced-order models for on-line aeroelastic predictions. Ph.D. dissertation, Stanford, USA (2010)
2. Astrid, P., et al.: Missing point estimation in models described by proper orthogonal decomposition. IEEE Trans. Autom. Control, **53**(10), 2237–2251 (2008)
3. Barrault, M., et al.: An 'empirical interpolation' method: application to efficient reduced-basis discretization of partial differential equations. C. R. Math. **339**(9), 667–672 (2004)
4. Bossavit, A.: Computational Electromagnetism: Variational Formulations, Complementarity, Edge Elements. Academic Press, San Diego (1998)
5. Bui-Thanh, T., Damodaran, M., Willcox, K.E. : Aerodynamic data reconstruction and inverse design using proper orthogonal decomposition. AIAA J. **42**, 1505–1516 (2004)
6. Chaturantabut, S., Sorensen, D.C.: Nonlinear model reduction via discrete empirical interpolation. SIAM J. Sci. Comput. **32**(5), 2737–2764 (2010)
7. Clenet, S., et al.: Model order reduction of non-linear magnetostatic problems based on POD and DEI methods. IEEE Trans. Magn. **50**, 33–36 (2014)
8. Cohen, A., DeVore, R.: Kolmogorov widths under holomorphic mappings. IMA J. Numer. Anal. (2015)
9. Dular, P., et al.: A general environment for the treatment of discrete problems and its application to the finite element method. IEEE Trans. Magn. **34**(5), 3395–3398 (1998)
10. Gyselinck, J.: Twee-Dimensionale Dynamische Eindige-Elementenmodellering van Statische en Roterende Elektromagnetische Energieomzetters. PhD thesis (1999)
11. Gyselinck, J., et al.: Calculation of eddy currents and associated losses in electrical steel laminations. IEEE Trans. Magn. **35**(3), 1191–1194 (1999)
12. Hiptmair, R., Xu, J.-C.: Nodal auxiliary space preconditioning for edge elements. In: 10th International Symposium on Electric and Magnetic Fields, France (2015)
13. Kolmogoroff, A.: Über die beste Annäaherung von Funktionen einer gegebenen Funktionenklasse. Ann. Math. Second Ser. **37**, 107–110 (1936)
14. Maday, Y., Patera, A., Turinici, G.: A priori convergence theory for reduced-basis approximations of single-parameter elliptic partial differential equations. J. Sci. Comput. **17**, 437–446 (2002)
15. Montier, L., et al: Robust model order reduction of a nonlinear electrical machine at start-up through reduction error estimation. In: 10th International Symposium on Electric and Magnetic Fields, France (2015)

16. Paquay, Y., Brüls, O., Geuzaine, C.: Nonlinear interpolation on manifold of reduced order models in magnetodynamic problems. IEEE Trans. Magn. **52**(3), 1–4 (2016)
17. Ryckelynck, D.: A priori hyperreduction method: an adaptive approach. J. Comput. Phys. **202**(1), 346–366 (2005)
18. Schilders, W., et al.: Model Order Reduction: Theory, Research Aspects and Applications, vol. 13. Springer, Berlin (2008)
19. Sirovich, L.: Turbulence and the dynamics of coherent structures. Part I: Coherent structures. Q. Appl. Math. **45**(3), 561–571 (1987)
20. Sorensen, D. Private discussions (2015)
21. Volkwein, S.: Proper orthogonal decomposition and singular value decomposition. Universität Graz/Technische Universität Graz. SFB F003-Optimierung und Kontrolle (1999)
22. Zlatko, D., Gugercin, S.: A New Selection Operator for the Discrete Empirical Interpolation Method–improved a priori error bound and extensions. SIAM J. Sci. Comput. **38**(5), A631–A648 (2016)